^{11}C-MK-8278 PET as a Tool for Pharmacodynamic Brain Occupancy of Histamine 3 Receptor Inverse Agonists

Koenraad J. Van Laere[1], Sandra M. Sanabria-Bohórquez[2], David P. Mozley[2], Donald H. Burns[2], Terence G. Hamill[2], Anne Van Hecken[3], Inge De Lepeleire[4], Michel Koole[1], Guy Bormans[5], Jan de Hoon[3], Marleen Depré[3], Kristine Cerchio[6], John Plalcza[6], Lingling Han[6], John Renger[7], Richard J. Hargreaves[2], and Robert Iannone[8]

[1]Division of Nuclear Medicine, University Hospital and KU Leuven, Leuven, Belgium; [2]Imaging, Merck Research Laboratories, West Point, Pennsylvania; [3]Center for Clinical Pharmacology, University Hospital Leuven, Leuven, Belgium; [4]Clinical Pharmacology, Merck Research Laboratories, Brussels, Belgium; [5]Laboratory of Radiopharmaceutical Chemistry, KU Leuven, Leuven, Belgium; [6]Clinical Biostatistics and Research Decision Sciences, Merck Research Laboratories, North Wales, Pennsylvania; [7]Neurosymptomatic Disorders, Merck Research Laboratories, West Point, Pennsylvania; and [8]Clinical Oncology, Merck Research Laboratories, North Wales, Pennsylvania

The histamine 3 (H3) receptor is a presynaptic autoreceptor in the central nervous system that regulates the synthesis and release of histamine and modulates the release of other major neurotransmitters. H3 receptor inverse agonists (IAs) may be efficacious in the treatment of various central nervous system disorders, including excessive daytime sleepiness, attention deficit hyperactivity disorder, Alzheimer disease, ethanol addiction, and obesity. **Methods:** Using PET and a novel high-affinity and selective radioligand ^{11}C-MK-8278, we studied the tracer biodistribution, quantification, and brain H3 receptor occupancy (RO) of MK-0249 and MK-3134, 2 potential IA drugs targeting cerebral H3 receptors, in 6 healthy male subjects (age, 19–40 y). The relationship among H3 IA dose, time on target, and peripheral pharmacokinetics was further investigated in 15 healthy male volunteers (age, 18–40 y) with up to 3 PET scans and 3 subjects per dose level. **Results:** The mean effective dose for ^{11}C-MK-8278 was 5.4 ± 1.1 μSv/MBq. Human brain kinetics showed rapid high uptake and fast washout. Binding potential values can be assessed using the pons as a reference region, with a test–retest repeatability of 7%. Drug RO data showed low interindividual variability per dose (mean RO SD, 2.1%), and a targeted 90% RO can be reached for both IAs at clinically feasible doses. **Conclusion:** ^{11}C-MK-8278 is a useful novel PET radioligand for determination of human cerebral H3 receptor binding and allows highly reproducible in vivo brain occupancy of H3-targeting drugs, hereby enabling the evaluation of novel compounds in early development to select doses and schedules.

Key Words: ^{11}C-MK-8278; PET; H3 receptor; receptor occupancy; inverse agonist; kinetic modeling

J Nucl Med 2014; 55:65–72
DOI: 10.2967/jnumed.113.122515

Histamine is an aminergic neurotransmitter that is localized in the central nervous system (CNS) and in peripheral tissues such as the gut, skin, and immune system. In the brain, histaminergic neurons originate in the tuberomammillary nucleus of the hypothalamus and project throughout the CNS, including the thalamus, hypothalamus, cerebral cortex, striatum, medulla oblongata, and spinal cord. There are 4 known G-protein–coupled histamine receptor subtypes (H1–H4). These serve multiple functions in the brain, particularly control of excitability and plasticity. Type 1 and 2 histamine receptor–mediated actions are mostly excitatory. The H3 receptor was discovered in 1983 and cloned at the end of the twentieth century (*1*) and is mainly expressed in the CNS. H3 receptors predominate in the basal ganglia, with the highest densities in the globus pallidus (*2*). The H3 receptor is a presynaptic inhibitory autoreceptor that regulates the synthesis and release of histamine and also modulates the release of several other neurotransmitters such as acetylcholine, norepinephrine, serotonin, dopamine, and γ aminobutyric acid. Like other G-protein–coupled receptors, H3 receptors signal constitutively, serving to tonically suppress histamine production at baseline. Agonist-induced signaling, such as that which occurs in the presence of elevated histamine levels, further suppresses histamine release.

Although a classic antagonist would interfere with histamine-mediated negative feedback, H3 receptor inverse agonists (IAs) have been demonstrated to decrease constitutive H3 signaling, thus enhancing histamine release and further potentiating histaminergic neurotransmission. Mutual interactions with these other transmitter systems form a network that links basic homeostatic and higher brain functions, including sleep–wake regulation, circadian and feeding rhythms, immunity, attention, learning, and memory (*3–9*). H3 receptor IAs may thus be efficacious in the treatment of various CNS disorders (*10,11*). Pitolisant was the first H3 IA to be introduced in the clinic. Its wake-promotion activity was evidenced in the excessive diurnal sleepiness of patients with narcolepsy, Parkinson disease, or obstructive sleep apnea/hypopnea, in which this activity is characterized by a mean decrease of the Epworth Sleepiness Scale by about 5 units (*11*). The procognitive activity of this novel class of drugs may also find therapeutic applications in dementia, schizophrenia, and attention deficit hyperactivity disorder. A potential role for H3 IAs is also advocated in obesity and ethanol addiction (*7,12*). In a study of sleep-deprived healthy male volunteers using the stimulant reference sleep deprivation model, a single 10-mg dose of MK-0249 was associated with alerting effects (*13*). In essential tremor, however, a recent human

Received Mar. 19, 2013; revision accepted Jul. 9, 2013.
For correspondence or reprints contact: Koenraad Van Laere, University Hospital Gasthuisberg Leuven, Herestraat 49, 3000 Leuven, Belgium.
E-mail: koen.vanlaere@uzleuven.be
Published online Nov. 21, 2013.
COPYRIGHT © 2014 by the Society of Nuclear Medicine and Molecular Imaging, Inc.

trial using MK-0249 did not find significant effects in tremor reduction even at high single dose doses of H3 IA administration (*14*).

Currently, there are few target-engagement biomarkers for H3 receptor blockade, and radionuclide imaging is the only technology available that can noninvasively quantify relationships between the administered dose of a drug, its plasma concentration levels, and its receptor occupancy (RO) in the brain. Optimizing the therapeutic window and selecting the proper dose of an investigational new drug to advance to proof-of-concept clinical trials can limit the testing of doses that may be too low to achieve efficacy or too high that saturate the H3 receptors in the brain and potentially lead to adverse events. This is especially important for H3 IAs in which excessive dosing may not add efficacy but could result in unwanted nighttime alerting.

In vivo imaging of the H3 receptor in humans has become possible using recently developed radioligands. Several selective IA tracers for H3 labeling with ^{11}C or ^{18}F have been discovered and evaluated in monkeys (*15*). Of these, ^{11}C-MK-8278 is a highly brain-penetrant and selective IA that allows dynamic imaging with fast washout from the brain. Other radioligands for the H3 receptor have been published, such as ^{11}C-GSK-189254—which is a highly potent, selective, and brain-penetrant receptor antagonist. The latter radiotracer can also be used to quantify H3 receptor availability but requires high specific activity (*16,17*) and has slow uptake kinetics; nevertheless, it was documented to be suitable for H3 RO determinations. Also, ^{11}C-AZ12807110 was recently used to assess H3 RO using the Lassen plot method (*18*).

The aim of the current study was to evaluate the biodistribution, dosimetry, and quantification of ^{11}C-MK-8278 in humans and to determine its utility in clinical occupancy studies of 2 novel histamine H3 IAs, MK-0249 (*13,14,19*) and MK-3134 (*20*). Open-label, 2-period, multipanel studies were done to investigate occupancies of single oral doses at the time of approximately maximum occupancy (approximate plasma T_{max}) in the target range of 50%–90% brain H3 RO. The RO relationship to pharmacokinetic parameters was investigated, and clinical and laboratory safety evaluations were performed. For MK-0249, single oral doses that demonstrated approximately 90% peak brain H3 RO were subsequently investigated over time to determine clearance from the brain compartment versus plasma concentration.

MATERIALS AND METHODS

Subjects

All human studies were conducted at a single site. In part I (tracer characterization and quantification), 6 healthy male volunteers participated (age range, 19–40 y; mean age ± SD, 26.3 ± 8.1 y). In part II (dosing studies with MK-0249 and MK-3134), in total 15 healthy, drug-free volunteers (age range, 18–40 y; mean age ± SD, 25.9 ± 6.9 y) participated. Each study part and panel was conducted with separate study populations. Volunteers were recruited in response to advertisements in the local University Hospital and community newspapers. No control was placed on socioeconomic status or educational level. All subjects underwent thorough physical examination, blood and urine testing, and high-resolution MR imaging T1 MPRAGE (magnetization prepared rapid gradient echo) and routine T2 imaging. Neuropsychiatric screening was performed using the Dutch version of the Patient Health Questionnaire (*21*). Exclusion criteria are given in the supplemental materials and methods (supplemental materials are available at http://jnm.snmjournals.org).

The study was approved by the Institution's Ethics Committee and performed in accordance with the latest version of the World Medical Association Declaration of Helsinki (http://www.wma.net/). Written informed consent was obtained from all the volunteers before the study.

^{11}C-MK-8278 Characteristics

MK-8278 is a potent IA at human histamine H3 receptors with an inhibition constant of 0.54 nM and log P (pH 7.4) of 2.2 (*15*). The structure of ^{11}C-MK-8278 is shown in Figure 1. The off-target activities of MK-8278 were evaluated in more than 170 receptor-binding or enzyme assays. MK-8278 is highly selective for histamine H3, with only weak off-target binding activities observed at 5-HT2 (51% inhibition at 10 μM) and 5-HT2A (62% inhibition at 10 μM), respectively. Autoradiographic studies of dog, rhesus, and human brain slices were performed using ^{3}H-MK-8278 as a radioligand and 10 mM R-a-methyl-(RAM)-histamine to determine nondisplaceable binding. In the rhesus monkey (Fig. 2), the highest binding densities were in the ventral pallidal and basal nuclei, nucleus accumbens, substantia nigra, and globus pallidus. Moderate binding was found in other parts of the brain, and the thalamic nuclei (ventral lateral) and brain stem exhibited minimal binding (*15*). MK-8278 is a poor substrate for human P-glycoprotein, with a transport ratio of 2.3, and shows low plasma protein binding (82% in humans). Toxicology data and tracer preparation details are given in the supplemental materials and methods.

Tracer specific activity in the study was 114 ± 112 GBq/μmol (range, 15–563 GBq/μmol) at the time of injection. The average MK-8278 mass dose given in the study per injection was 2.1 ± 1.8 μg,

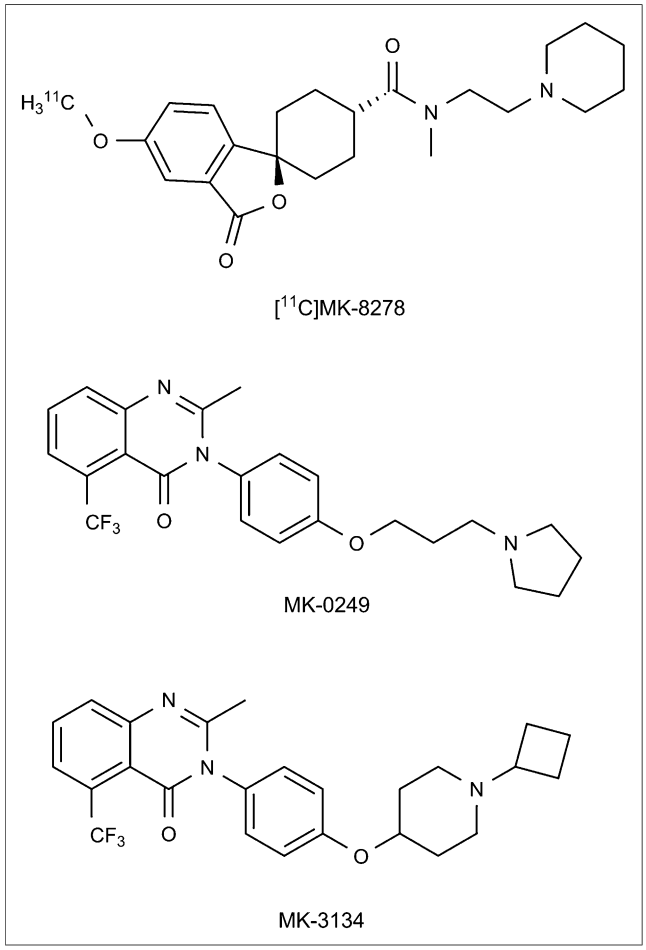

FIGURE 1. Chemical structures of ^{11}C-MK-8278, MK-0249, and MK-3134.

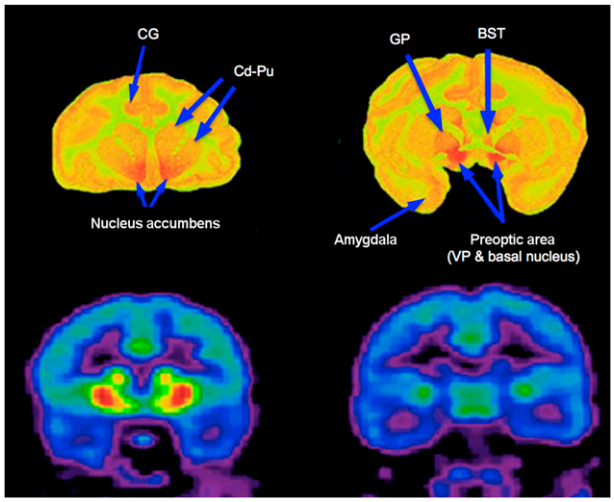

FIGURE 2. Autoradiography of ^{11}C-MK-8278 imaging in rhesus monkey versus summed image (0–100 min) in human subject. Coronal slices through level of nucleus accumbens and globus pallidus are shown. BST = bed stria terminalis; Cd-Pu = caudate-putamen; CG = cingulate gyrus; GP = globus pallidus; VP = ventropallidal.

whereas the maximum total mass dose given for any individual was 13.6 μg (mean total mass dose given for multiple administrations, 5.3 ± 3.6 μg).

Imaging Procedure

For whole-body biodistribution scanning (part IA), 3 subjects underwent 8 serial whole-body PET scans for 2 h after bolus injection of 307 ± 25 MBq of ^{11}C-MK-8278. PET scans were performed on an ECAT EXACT HR+ (Siemens).

Second, ^{11}C-MK-8278 brain kinetics and test–retest (*T-RT*) repeatability were evaluated in 3 other healthy male subjects (part IB). Dynamic brain scans were obtained on a HiRez Biograph 16 LSO (lutetium oxyorthosilicate)–enabled PET/CT (16 CT slice) camera (Siemens) in 3-dimensional (3D) mode. The subject's head was restrained using a vacuum holder cushion to reduce movement artifacts during the scan. Baseline sensory conditions (dimmed room lighting, reduced noise) were imposed throughout the scans.

After the subject was positioned in the scanner, a bolus of approximately 288 ± 16 MBq was injected intravenously, with the simultaneous start of a dynamic emission scan. This dynamic scan consisted of 24 frames with progressive increase in frame duration (4 × 15, 4 × 60, 6 × 150, 8 × 300, and 4 × 600 s) and a total duration of 100 min.

Images were reconstructed with a standard 3D filtered-backprojection algorithm, including scatter and measured attenuation correction (^{68}Ge source for the biodistribution studies and an 11-mA CT scan [0.04 mSv/head scan] for PET/CT imaging), and were corrected for decay, random coincidences, and dead time.

In part IB, each of the subjects underwent 2 PET scans on the same day with an interval of 3–4 h. In this part, arterial blood was withdrawn for ^{11}C-MK-8278 and metabolites to generate an arterial input function curve. Details on arterial blood sampling and metabolite analysis are given in the supplemental material and methods.

All subjects underwent high-resolution MR imaging, with T1-weighted 3D MPRAGE and T2-weighted imaging, on a 1.5-T Vision Scanner (Siemens). Parameters for the T1 3D MPRAGE sequence were relaxation time, 0 ms; echo time, 4 ms; flip angle, 12°; inversion time, 300 ms; matrix, 256 × 256; and 160 contiguous sagittal slices of 1 mm.

For H3 RO measures in part II, 15 healthy male volunteers (age, 18–40 y) participated. A bolus over 30 s of 272 ± 20 MBq (range, 195–309 MBq) of ^{11}C-MK-8278 was injected intravenously, and a 100-min dynamic emission scan was simultaneously started. No arterial blood sampling was performed in the occupancy studies because the pons was suitable as a reference tissue. Subjects underwent all scanning within a time period of on average 2 wk (maximum range, 2 mo). PET scans were obtained 6 h after dosing of MK-0249 and MK-3134. This time point approximates the time of the expected plasma maximal concentration (C_{max}) for both compounds. For MK-0249, additional scans were obtained 27 h postdose.

Safety Assessment

Safety and tolerability were assessed throughout the study by monitoring clinical adverse experiences, physical examinations, vital sign recording, 12-lead electrocardiograms, and multiple laboratory safety tests.

Data Analysis

For dosimetry calculations, 3D source organs were delineated in the brain, lungs, kidneys, liver, bladder, prostate, and pancreas using PMOD 2.9 (PMOD Inc.). Time-integrated activity coefficients (formerly called residence times) were derived from the time–activity profiles. Individual organ doses and effective doses were determined using the OLINDA/EXM software (version 1.0; Vanderbilt University), with the same approach and curve-fitting procedures as applied previously (*22*).

For kinetic modeling of the *T-RT* scans, the ^{11}C-MK-8278 plasma input function was estimated using total activity counts and the relative plasma fraction measured in arterial samples. A PET template was obtained using a baseline ^{11}C-MK-8278 PET image by summing all frames in the acquisition. The PET template and the MR image were aligned using SPM99 (http://www.fil.ion.ucl.ac.uk/spm). Then, using the MR imaging scans for anatomic delineation, regions of interest were drawn on the caudate, putamen, thalamus, mid brain, cingulate gyrus, insula, occipital cortex, cerebellum, and pons, with the Montreal Neurologic Institute DISPLAY software (http://www.bic.mni.mcgill.ca/software). Subsequent baseline/RO scans obtained in a subject were coregistered to the respective PET template before generation of the time–activity curves.

Tissue time–activity curves (TAC) were obtained by projecting the defined regions of interest onto all frames of the dynamic PET scans and expressed in SUV (standardized uptake value) using each subject's weight and the corresponding injected tracer dose:

$$TAC\,(\mathrm{SUV}) = TAC\,(\mathrm{MBq}) \times 1{,}000 \times \text{subject's weight (kg)/injected dose (MBq)}.$$

Time–activity curves and all subsequent analyses were performed using in-house–developed analysis software written in Matlab (The MathWorks).

For RO determination, all image data analysis was conducted under masked conditions to dose and postdose scan time. H3 receptor availability was estimated using binding potential (BP_{ND}) with the pons as reference. Drug occupancy at T h after drug administration (RO[T]) was calculated as:

$$\mathrm{RO}(T) = [BP_{ND}(\mathrm{baseline}) - BP_{ND}(T)]/BP_{ND}(\mathrm{baseline}) \times 100\%.$$

The nondisplaceable distribution volume (V_{ND}) was considered as a constant in all gray matter regions. RO was related to the dose and the average concentration of the H3 IAs during the scanning session.

A 2-parameter hill curve was fit through the occupancy versus dose or plasma concentration, based on the following equation:

$$\%RO = Occ_{50}^{h}/\left(Occ_{50}^{h} + x^{h}\right),$$

where h is the Hill coefficient, x is the dose or drug plasma concentration, and Occ_{50} is the x-value corresponding to 50% occupancy value.

Single-Dose H3 IA Studies

MK-0249 and MK-3134 both have a quinazolinone structure (Fig. 1) and have been used in several clinical studies (*13,14,19*). Both compounds have a nanomolar affinity for H3 receptors and are highly specific for H3 receptors (inhibition constant is >10 μM for H1, H2, and H4, and no other off-target activities below 1 μM). The pharmacologic dose-selection rationale for the occupancy studies and pharmacokinetic plasma analysis methods are given in the supplemental materials and methods.

RESULTS

Biodistribution and Dosimetry

An effective dose of 5.4 ± 1.1 μSv/MBq was found. Table 1 summarizes the individual organ doses and their variance between subjects. Figure 3 shows exemplary dynamic whole-body scans, indicating a combination of hepatobiliary and urinary excretion of the tracer and rapid brain uptake. The highest individual organ radiation-absorbed dose was estimated to be in the pancreas (40.2 ± 13.0 μGy/MBq). The effective dose was consistent with the values found in preclinical studies of nonhuman primates with this tracer (4.8 μSv/MBq) and is in the typical range of other ^{11}C-labeled radiopharmaceuticals (*23*). Further activity for the study (kinetic modeling and occupancy determination) was set at 300 MBq per injection, based on this measured effective radiation dose (1.63 mSv per scan) and the obtained specific activity (maximum mass, 6.4 μg).

TABLE 1
Radiation Dosimetry of ^{11}C-MK-8278 in 3 Healthy Young Male Volunteers

Target organ	Mean (μGy/MBq)	Mean (mGy/300 MBq)	Variance (%)
Pancreas	40.2	12.1	32.3
Small intestine	16.4	4.91	2.3
Lungs	14.4	4.33	31.4
Liver	14.4	4.32	16.0
Kidneys	13.6	4.08	22.4
Spleen	11.1	3.33	51.6
Thyroid	6.2	1.87	26.7
Urinary bladder wall	5.0	1.49	9.7
Gallbladder wall	4.8	1.44	30.5
Heart wall	4.5	1.36	32.0
Brain	3.9	1.16	6.9
Upper large intestine wall	3.4	1.02	4.6
Adrenals	3.0	0.91	12.5
Ovaries	2.4	0.73	6.6
Stomach wall	2.4	0.73	12.6
Uterus	2.4	0.71	7.4
Total body (remainder)	2.3	0.70	10.0
Osteogenic cells	2.1	0.63	18.9
Red marrow	2.1	0.63	20.2
Lower large intestine wall	2.0	0.59	8.6
Thymus	1.6	0.47	11.4
Muscle	1.5	0.44	10.9
Breasts	1.4	0.41	11.5
Skin	1.0	0.30	12.7
Testes	1.0	0.30	16.0
Effective dose	5.4 (μSv/MBq)	1.63 (mSv/300 MBq)	19.8

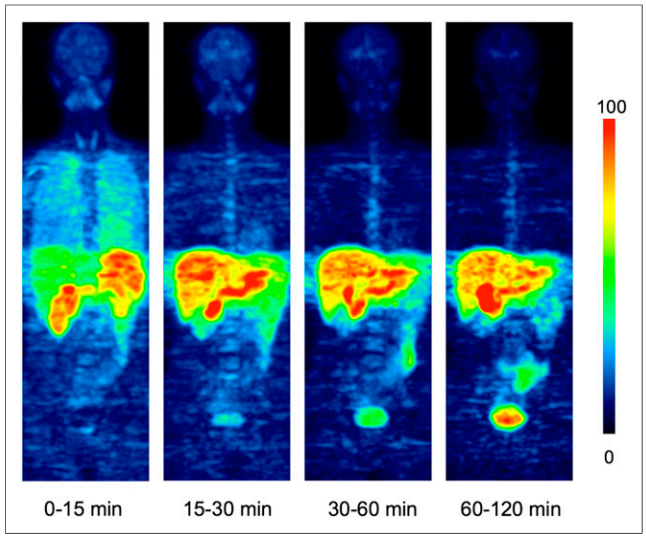

FIGURE 3. Dynamic human biodistribution of ^{11}C-MK-8278. Maximal-intensity projections at consecutive time intervals (normalized on image maximum).

Kinetic Modeling and *T-RT* Repeatability

The cerebral tracer uptake is shown in Figure 4 and the time–activity curves in Figure 5. The highest uptake was observed in the striatum, followed by the cingulate gyrus, mid brain, and thalamus. Lower uptake was observed in cortical regions and cerebellum. The lowest uptake was observed in the pons. H3 receptor availability could be estimated using a 1-compartment model with the metabolite-corrected tracer arterial input function. With this model, an index of receptor availability was estimated from the total distribution volume, $V_T = K_1/k_2$ (*24*). In addition to this, a simplified reference tissue model was applied to estimate another index of receptor availability, BP_{ND} (*25*), using the pons as the reference tissue. Although it has not been shown that the pons is completely devoid of H3 receptors, the shape of the pons curve in Figure 2 (early peak activity and fast washout) suggests that the H3 receptor density in this region can be considered negligible. Table 2 summarizes the regional V_T and BP_{ND} values for ^{11}C-MK-8278 in healthy volunteers.

The time stability of these outcome measures was evaluated between 60 and 100 min of data acquisition. A scan length of

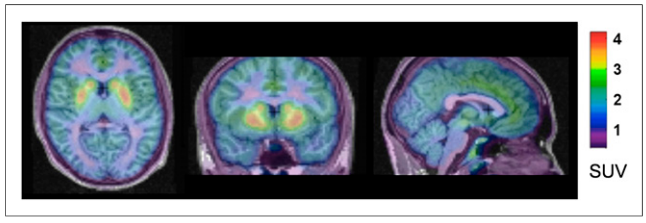

FIGURE 4. Orthogonal sections of summed late-time images (60–80 min) of ^{11}C-MK-8278 in human brain.

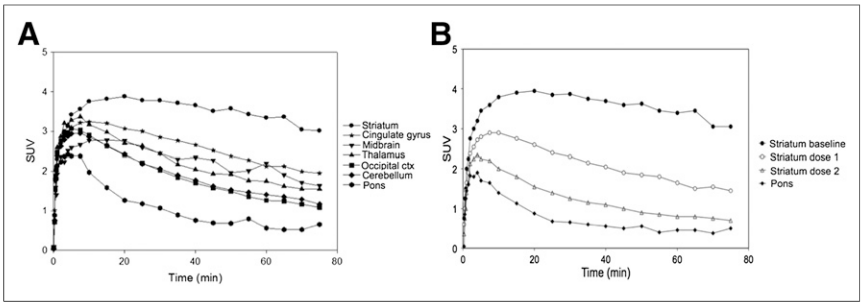

FIGURE 5. ^{11}C-MK-8278 time–activity curves in brain of male, healthy volunteer under baseline condition (A) and after dosing with 2 different doses of MK-0249 (B).

80 min was found adequate for estimating H3 receptor availability using both the 1-tissue-compartment model with a plasma input function and the reference tissue approach (supplemental results).

T-RT repeatability for V_T and BP_{ND} with scan data to 80 min was determined and defined as 100 × abs[*T-RT*]/*T*. The *T-RT* repeatability using the 1-tissue-compartment model with an input function was 16.3% ± 6.0% in the putamen and 20.1% ± 4.2% in the caudate. This fairly large value could be explained by low statistics in the determination of the plasma curve estimation (total counts and metabolite correction) at time points above 60 min. *T-RT* values were smaller in all the other examined regions (mean *T-RT*, 5.0% ± 4.1%; univariate ANOVA showed no significant differences between V_T *T-RT* values between subjects, $P > 0.5$). The *T-RT* repeatability for BP_{ND} estimates in the striatum using the pons as a reference region was 6.3% ± 4.4% in the putamen and 2.9% ± 4.1% in the caudate. *T-RT* values of BP_{ND} were below 10% in all the examined regions (mean *T-RT*, 4.2% ± 2.7%; univariate ANOVA showed no significant differences between V_T *T-RT* values between subjects, $P > 0.6$). Supplemental Figure 2 shows *T-RT* values for BP_{ND} (converted to distribution volume ratio [DVR] for comparison to the V_T *T-RT* values). For the ensuing occupancy measurements, BP_{ND} values were used, based on data with 80-min acquisition.

H3 RO by Single Oral Doses of MK-0249 and MK-3134

Examples of baseline and blocked scans are shown in Figure 6 for a subject who received 2.5 or 12.5 mg of MK-0249, imaged 6 and 27 h postdose. The combined central H3 RO data of MK-0249 and MK-3134 measured in the striatum (region of highest tracer uptake) using BP_{ND} with the pons as a reference region are summarized in Figure 7 as a function of drug dosage (Fig. 7A) and drug plasma concentration (Fig. 7B). For drug dosage, the fitted Hill coefficient *h* and Occ_{50} were 0.8 and 1.2 mg for MK-0249 and 1 and 0.6 mg for MK-3134, respectively. For drug plasma concentration, *h* and Occ_{50} were 0.72 and 1.5 nM for MK-0249 and 1 and 0.32 nM for MK-3134, respectively.

Table 3 provides a summary of striatal RO data for both compounds. RO values were consistent between subjects, with a mean SD of the 3-dose point measures of 2.1% ± 1.7% (range, 0.6%–7.6%), which is well within the estimate of repeatability of the BP_{ND} measurement (see above). BP_{ND} changes in all brain regions of interest, including extrastriatal areas, were similar, indicating that occupancy is homogeneous throughout the brain.

The second part of the trial for MK-0249 included PET scanning at time points well after T_{max} to assess RO during the declining pharmacokinetic phase. Supplemental Figure 3 shows the dynamic occupancy over time for MK-0249. The brain occupancy half-life was 51.2 h for MK-0249 (Supplemental Fig. 3A), which is longer than the plasma concentration half-life of 18.6 h (Supplemental Fig. 3B). However, RO during the rising and declining plasma concentration phases (6 and 27 h postdose) suggest that brain RO is highly related to plasma concentration—that is, the longer brain half-life could be explained by brain concentrations that exceeded saturation rather than hysteresis

Safety Assessment

For both IA compounds, the study was conducted in an open-label fashion. Clinical adverse experiences were reported to be mild to moderate in intensity and resolved spontaneously. No serious adverse events occurred. Adverse event details are given in the supplemental results.

DISCUSSION

The histaminergic system is widely disseminated in the nervous system and may influence the regulation of multiple functions including but not limited to arousal, satiety, attention, and cognition. Signaling through the H3 receptor activates G proteins, which inhibit adenylate cyclase production and reduce cyclic adenosine monophosphate (cAMP), protein kinase A, and cAMP-responsive element-binding proteins. A principal effect of cAMP-responsive element-binding protein modulation of gene expression is reduced levels of histamine. H3 receptors are also known to modulate the release of other neurotransmitters. Like some other G-protein–coupled receptors, H3 receptors signal constitutively, serving to constitutively suppress neurotransmitter production. Agonist-induced signaling, such as that which occurs in the presence of elevated histamine levels,

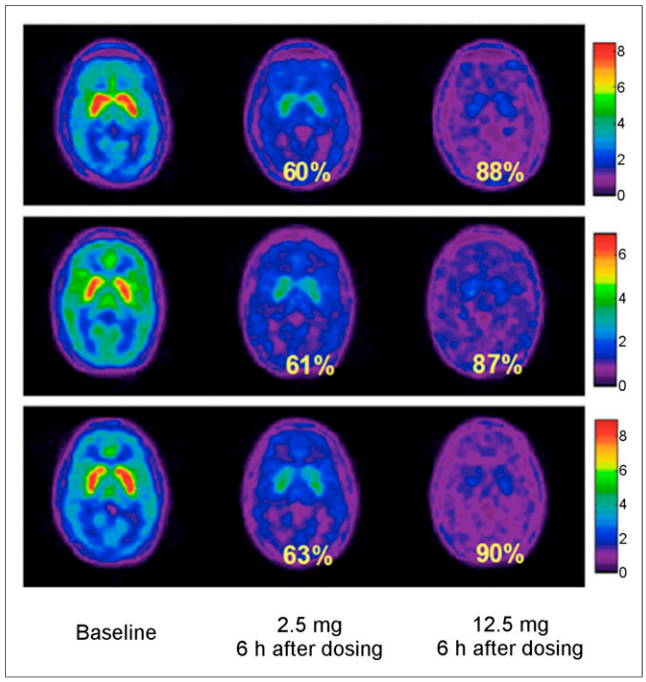

FIGURE 6. Transverse images at level of striatum for 3 consecutive healthy volunteers, showing RO changes for MK-0249 with 2.5- and 12.5-mg administration, 6 h postdose. Color scale indicates SUVs.

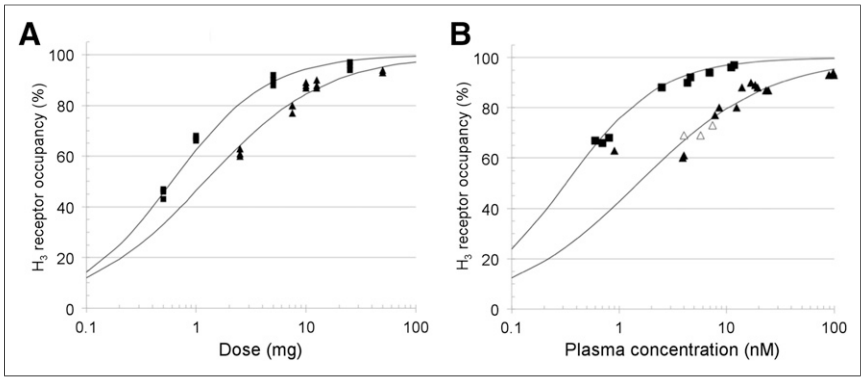

FIGURE 7. (A) Occupancy versus dose relationship for MK-0249 (▲) and MK-3134 (■) and fitted Hill curves. (B) Occupancy versus plasma concentration relationship for MK-0249 (▲, 6 h postdose; △, 27 h postdose) and for MK-3134 (■, 6 h postdose).

may further suppress histamine release. Although a classic antagonist would interfere with histamine-mediated negative feedback, H3 receptor IAs have been demonstrated to decrease constitutive H3 receptor signaling, thus releasing tonic inhibition of neurotransmitter release and allowing potentiating effects of neurotransmission.

This study demonstrates the utility of PET scanning to characterize the pharmacodynamic occupancy profile of different potential compounds for the H3 target to inform the rational selection of optimal dosing for future clinical evaluations. In vivo H3 receptor brain distribution using ^{11}C-MK-8278 was in qualitative agreement with autoradiography data in humans (*15*) and that reported for ^{11}C-GSK189254 (*16*), indicating suitability of the ^{11}C-MK-8278 for demonstrating H3 receptor sites in the brain in vivo. The development of radioligands for PET imaging of receptors in the CNS is a demanding task, and although binding has been demonstrated for many radioligands for the H3, only a few are suitable for applied quantitative studies. Clinical studies with ^{11}C-GSK189254 showed slow uptake of the tracer into the brain (*16*), and over the time course of the PET scan, equilibrium was not achieved. Furthermore, it was not possible to fit compartmental models to brain regions with high levels of tracer binding, and thus to quantify H3 receptor availability, high specific activity was necessary. The development of ^{11}C-MK-8278 constitutes a major step in the characterization of the histaminergic system in human and animal CNSs. In vivo occupancy determination allows for demonstration of target engagement and can aid in titration of dose regimens for subsequent clinical trials, compared with pharmacokinetic profiling alone. The assessment of target engagement is critical in bridging from preclinical experiments to the clinic to optimize the therapeutic margin. Moreover, occupancy may also serve as a correlate of pharmacodynamic and safety parameters, as has been assessed extensively with other systems such as the dopamine D_2 receptor (*26*). Because there is no need for arterial sampling to reliably quantify the binding potential for ^{11}C-MK-8278 with good *T-RT* variability (<4%), this suggests this tracer may be a valuable tool for quantification of H3 receptor availability in proof-of-principle experiments in various relevant diseases such as Alzheimer disease (*6,27*) and sleep disorders (*4,28*).

Comparison of RO during the rising and declining plasma concentration phases (6 and 27 h postdose) suggest that brain RO is highly related to plasma concentration—that is, there is no hysteresis. Having established the brain RO to plasma concentration relationship for MK-0249 and MK-3134, dose and schedule in clinical trials could be informed by the results of these studies to match a target RO profile between dosing intervals. The clinical development of MK-3134 and MK-0249, however, has been halted for strategic reasons as determined by Merck. Furthermore, PET could be used to select among these compounds and others in development with different pharmacokinetic profiles across indications to optimize therapeutic effects when needed most and potentially minimize unwanted effects such as nighttime alerting (*18*).

TABLE 2
Distribution Volume V_T and BP_{ND} ^{11}C-MK-8278 in Healthy Volunteers

	^{11}C-MK-8278			
	V_T		BP_{ND}	
Organ	Mean	SD	Mean	SD
Striatum	17.1	1.9	2.16	0.07
Thalamus	8.8	0.9	0.86	0.08
Mid brain	9.8	1.2	1.00	0.09
Frontal	8.4	0.7	0.81	0.13
Anterior cingulate gyrus	10.2	1.1	1.15	0.21
Posterior cingulate gyrus	8.9	1.1	0.92	0.26
Parietal	7.9	0.8	0.69	0.08
Insula	8.6	0.8	0.84	0.12
Temporal	7.7	0.7	0.66	0.09
Occipital	7.0	0.5	0.53	0.08
Cerebellum	7.4	0.5	0.64	0.13
Pons	4.5	0.5		
White matter	3.7	0.4		

CONCLUSION

The current study shows that ^{11}C-MK-8278 PET imaging can be used successfully to characterize target engagement by brain RO across plasma concentrations of 2 H3 receptor IAs. Dynamic ^{11}C-MK-8278 PET using the pons as a reference region is able to provide noninvasive, accurate and reproducible estimates of receptor availability (BP_{ND}) for clinical in vivo proof-of-mechanism studies.

DISCLOSURE

The costs of publication of this article were defrayed in part by the payment of page charges. Therefore, and solely to indicate this fact, this article is hereby marked "advertisement" in accordance with 18 USC section 1734. The Leuven University Hospital groups obtained financial sponsoring from Merck & Co, Inc., for carrying out the human PET studies. Koenraad J. Van Laere is Senior Clinical Investigator for the Fund for Scientific Research, Flanders, Belgium, and is Principal Investigator for study grants from Merck Inc., GE Healthcare, and Johnson & Johnson. Sandra M. Sanabria-Bohórquez, Kristine Cerchio, John Plalcza, Lingling Han, John Renger, David P. Mozley, Donald H. Burns, Terence G. Hamill, Richard J. Hargreaves, Robert Iannone, and Inge De Lepeleire are employees of Merck Inc. No other potential conflict of interest relevant to this article was reported.

TABLE 3
Activity, Dosing, and Striatal Occupancy Data for MK-0249 and MK-3134

Subject no.	Activity (MBq)	Dose (mg)	H3 RO (%, striatum)	Plasma level (nM)	Time scan (h postdose)
MK-0249					
Panel A					
1	273	Baseline	—	—	—
2	234	Baseline	—	—	—
3	259	Baseline	—	—	—
1	296	2.5	60	3.9	6
2	275	2.5	61	4.0	6
3	261	2.5	63	0.9	6
1	273	12.5	88	19.5	6
2	265	12.5	87	24.3	6
3	282	12.5	90	16.9	6
Panel B					
4	298	Baseline	—	—	—
5	282	Baseline	—	—	—
6	265	Baseline	—	—	—
4	286	7.5	80	8.5	6
5	288	7.5	80	12.4	6
6	256	7.5	77	7.8	6
4	269	50	94	97.9	6
5	274	50	93	99.4	6
6	267	50	93	89.7	6
Panel E					
13	259	Baseline	—	—	—
14	280	Baseline	—	—	—
15	278	Baseline	—	—	—
13	264	10	87	23.3	6
14	275	10	88	13.8	6
15	277	10	89	18.5	6
13	261	10	73	7.4	27
14	284	10	69	4.0	27
15	256	10	69	5.7	27
MK-3134					
Panel A					
1	267	Baseline	—	—	—
2	274	Baseline	—	—	—
3	309	Baseline	—	—	—
1	292	1	69	0.8	6
2	304	1	66	0.7	6
3	296	1	67	0.6	6
1	273	5	89	4.3	6
2	273	5	92	4.6	6
3	296	5	88	2.5	6
Panel B					
4	285	Baseline	—	—	—
5	293	Baseline	—	—	—
6	302	Baseline	—	—	—
4	289	0.5	47	BLQ	6
5	264	0.5	46	BLQ	6
6	256	0.5	43	BLQ	6
4	283	25	94	6.9	6
5	263	25	97	11.8	6
6	306	25	96	11.0	6

BLQ = below level of quantification.

ACKNOWLEDGMENTS

We acknowledge the skilled contributions of Stijn Dirix, the PET radiopharmacy group, and personnel of the Center for Clinical Pharmacology.

REFERENCES

1. Lovenberg TW, Roland BL, Wilson SJ, et al. Cloning and functional expression of the human histamine H3 receptor. *Mol Pharmacol.* 1999;55:1101–1107.
2. Martinez-Mir MI, Pollard H, Moreau J, et al. Three histamine receptors (H1, H2 and H3) visualized in the brain of human and non-human primates. *Brain Res.* 1990;526:322–327.

3. Haas HL, Sergeeva OA, Selbach O. Histamine in the nervous system. *Physiol Rev.* 2008;88:1183–1241.
4. Parmentier R, Anaclet C, Guhennec C, et al. The brain H3-receptor as a novel therapeutic target for vigilance and sleep-wake disorders. *Biochem Pharmacol.* 2007;73:1157–1171.
5. Stocking EM, Letavic MA. Histamine H3 antagonists as wake-promoting and pro-cognitive agents. *Curr Top Med Chem.* 2008;8:988–1002.
6. Brioni JD, Esbenshade TA, Garrison TR, Bitner SR, Cowart MD. Discovery of histamine H3 antagonists for the treatment of cognitive disorders and Alzheimer's disease. *J Pharmacol Exp Ther.* 2011;336:38–46.
7. Passani MB, Blandina P, Torrealba F. The histamine H3 receptor and eating behavior. *J Pharmacol Exp Ther.* 2011;336:24–29.
8. Raddatz R, Tao M, Hudkins RL. Histamine H3 antagonists for treatment of cognitive deficits in CNS diseases. *Curr Top Med Chem.* 2010;10:153–169.
9. Hough LB, Rice FL. H3 receptors and pain modulation: peripheral, spinal, and brain interactions. *J Pharmacol Exp Ther.* 2011;336:30–37.
10. Gemkow MJ, Davenport AJ, Harich S, Ellenbroek BA, Cesura A, Hallett D. The histamine H3 receptor as a therapeutic drug target for CNS disorders. *Drug Discov Today.* 2009;14:509–515.
11. Schwartz JC. The histamine H3 receptor: from discovery to clinical trials with pitolisant. *Br J Pharmacol.* 2011;163:713–721.
12. Panula P, Nuutinen S. H3 receptor miniseries: histamine and H3 receptor in alcohol-related behaviors. *J Pharmacol Exp Ther.* 2011;336:9–16.
13. Iannone R, Palcza J, Renger JJ, et al. Acute alertness-promoting effects of a novel histamine subtype-3 receptor inverse agonist in healthy sleep-deprived male volunteers. *Clin Pharmacol Ther.* 2010;88:831–839.
14. Zoethout RW, Iannone R, Bloem BR, et al. The effects of a novel histamine-3 receptor inverse agonist on essential tremor in comparison to stable levels of alcohol. *J Psychopharmacol.* 2012;26:292–302.
15. Hamill TG, Sato N, Jitsuoka M, et al. Inverse agonist histamine H3 receptor PET tracers labelled with carbon-11 or fluorine-18. *Synapse.* 2009;63:1122–1132.
16. Ashworth S, Rabiner EA, Gunn RN, et al. Evaluation of ^{11}C-GSK189254 as a novel radioligand for the H3 receptor in humans using PET. *J Nucl Med.* 2010;51:1021–1029.
17. Plisson C, Gunn RN, Cunningham VJ, et al. ^{11}C-GSK189254: a selective radioligand for in vivo central nervous system imaging of histamine H3 receptors by PET. *J Nucl Med.* 2009;50:2064–2072.
18. Jucaite A, Takano A, Bostrom E, et al. AZD5213: a novel histamine H3 receptor antagonist permitting high daytime and low nocturnal H3 receptor occupancy, a PET study in human subjects. *Int J Neuropsychopharmacol.* 2013;16:1231–1239.
19. James LM, Iannone R, Palcza J, et al. Effect of a novel histamine subtype-3 receptor inverse agonist and modafinil on EEG power spectra during sleep deprivation and recovery sleep in male volunteers. *Psychopharmacology (Berl).* 2011;215:643–653.
20. Cho W, Maruff P, Connell J, et al. Additive effects of a cholinesterase inhibitor and a histamine inverse agonist on scopolamine deficits in humans. *Psychopharmacology (Berl).* 2011;218:513–524.
21. Spitzer RL, Kroenke K, Williams JB. Validation and utility of a self-report version of PRIME-MD: the PHQ primary care study. Primary Care Evaluation of Mental Disorders. Patient Health Questionnaire. *JAMA.* 1999;282:1737–1744.
22. Van Laere K, Ahmad RU, Hudyana H, et al. Human biodistribution and dosimetry of ^{18}F-JNJ42259152, a radioligand for phosphodiesterase 10A imaging. *Eur J Nucl Med Mol Imaging.* 2013;40:254–261.
23. Gatley SJ. Estimation of upper limits on human radiation absorbed doses from carbon-11-labeled compounds. *J Nucl Med.* 1993;34:2208–2215.
24. Innis RB, Cunningham VJ, Delforge J, et al. Consensus nomenclature for in vivo imaging of reversibly binding radioligands. *J Cereb Blood Flow Metab.* 2007;27:1533–1539.
25. Lammertsma AA, Hume SP. Simplified reference tissue model for PET receptor studies. *Neuroimage.* 1996;4:153–158.
26. Kapur S, Zipursky RB, Remington G. Clinical and theoretical implications of 5-HT2 and D2 receptor occupancy of clozapine, risperidone, and olanzapine in schizophrenia. *Am J Psychiatry.* 1999;156:286–293.
27. Medhurst AD, Roberts JC, Lee J, et al. Characterization of histamine H3 receptors in Alzheimer's Disease brain and amyloid over-expressing TASTPM mice. *Br J Pharmacol.* 2009;157:130–138.
28. Lin JS, Sergeeva OA, Haas HL. Histamine H3 receptors and sleep-wake regulation. *J Pharmacol Exp Ther.* 2011;336:17–23.